One-Step Fabrication of a New Outstanding Rutile TiO2 Nanoparticles/Anthracite Adsorbent: Modeling and Physicochemical Interpretations for Malachite Green Removal

H.S. Ramadan, Rabea A.M. Ali, Mohamed Mobarak, Michael Badawi, Ali Q. Selim, Essam A. Mohamed, Adrián Bonilla-Petriciolet, Moaaz K. Seliem

One-step fabrication of a new outstanding rutile TiO_2 nanoparticles/anthracite adsorbent: Modeling and physicochemical interpretations for malachite green removal

H.S. Ramadan[a], Rabea A.M. Ali [a], Mohamed Mobarak [b], Michael Badawi [c,*], Ali Q. Selim [a], Essam A. Mohamed [a] , Adrián Bonilla-Petriciolet [d], Moaaz K. Seliem [a, *]

[a] Faculty of Earth Science, Beni-Suef University, 62511 Egypt

[b] Physics Department, Faculty of Science, Beni-Suef University, 62511 Egypt

[c] Laboratoire de Physique et Chimie Théoriques, UMR 7019 – CNRS, Université de Lorraine, France

[d] Instituto Tecnológico de Aguascalientes, Aguascalientes 20256, Mexico

Corresponding authors: michael.badawi@univ-lorraine.fr; debakyms@yahoo.com

Abstract

In this study, a facile method was developed to synthesize a new composite via the impregnation of rutile (TiO_2) nanoparticles (Rt) into H_2O_2–modified anthracite (MAn). This new rutile(TiO_2)/modified anthracite (Rt/MAn) adsorbent was characterized and employed as an outstanding and cost‐effective material to remove malachite green (MG) dye at 25 - 55 °C. This adsorbent displayed the highest removal efficiency (96.2 %) as compared to its individual components MAn (49.8 %) and Rt (71.4 %) at pH 8.0. The experimental adsorption of MG onto Rt/MAn at equilibrium were satisfactorily fitted to the Freundlich equation and a multilayer statistical physics model at all tested temperatures. The physicochemical parameters (steric and energetic) related to a multilayer adsorption

were calculated and interpreted to understand the adsorption mechanism. The theoretical number of adsorbed MG dye molecules per functional group (n) varied from 0.94 to 1.60 indicating a multi-docking adsorption mechanism. The adsorption capacity of MG at saturation (Q_{sat}) increased from 513 to 740 mg/g at 25 and 55 °C and was primarily caused by the density of Rt/MAn functional groups (i.e., the D_M parameter). MG adsorption energy with Rt/MAn varied from 13.87 to 29. 96 kJ/mol and was governed by physical interactions. The tested adsorbent was easily reactivated by the dye desorption and reused up to five cycles where it retained more than 80 % of MG adsorption capacity even after the 5th adsorption-desorption cycle. These results demonstrated that Rt/MAn is an effective adsorbent to remove MG, thus offering outstanding adsorption capacities largely beyond the current state of the art (up to 740 mg/g) and its application could be extended for the adsorption of other organic pollutants from wastewaters.

Keywords: Anthracite, rutile nanoparticles, malachite green, adsorption, statistical physics modeling, desorption.

Corresponding authors

Michael Badawi: michael.badawi@univ-lorraine.fr

Moaaz K. Seliem: debakyms@yahoo.com

1. Introduction

Numerous industrial processes, which are associated to the production of different colored products as leather, silk, wool and paper, generate effluents containing high residual amounts of dyes and, consequently, they contribute to increase the concentration of these organic pollutants in water bodies and environment [1, 2]. Former studies indicated that dyes are stable chemical compounds and can remain as pollutants in the aquatic environment for extended times [3]. Organic pollutant discharge into the water sources without a preliminary treatment represents a significant hazard for living organisms and human beings due their carcinogenic and toxic properties [4]. Thus, the finding an appropriate method for cleaning the polluted water to be reused in different fields of life is mandatory. Based on different benefits such as high efficiency, easy regeneration and low-cost that have been listed in several published articles, the water purification through adsorption is recommended as compared to biological, coagulation, membrane or precipitation techniques [5-9].

Malachite Green (MG) is a basic dye generally employed to color paper, silk, cotton, and wool products. From the water depollution perspective, this synthetic dye is difficult to be removed from aqueous solutions [10]. Note that a chronic exposure to MG can cause harmful effects in the kidney, gill, liver and gonads. The removal of this synthetic dye is a priority to reduce environmental pollution and health risks for population [11]. Therefore, numerous materials such as bentonite [12], natural zeolite [13], activated serpentine [8], carbon [14], activated carbon [15], activated rice husk [16], TiO_2 nanoparticles [17], and MCM–48/rice husk composite [18] were utilized as MG adsorbents. However, finding effective adsorbents for MG dye with outstanding adsorption capacities and short time to

achieve the adsorption equilibrium is still a remarkable issue. In addition, interpretation of the physicochemical parameters related to both of the experimental and theoretical studies can provide new insights into MG adsorption mechanism at the molecular level.

Several studies confirmed that utilizing carbon–rich materials as adsorbents is a competitive, environmentally friendly and low-cost approach to remove different water contaminants [7, 19]. The functional groups of these carbonaceous materials can be tailored to form different interactions with water pollutants thus improving their adsorption capacities [7, 19]. Anthracite, the used carbon-rich material, is characterized by the highest carbon concentration (more than 86 %) and thus, it is considered as a high grade coal [7], which makes it directly usable in the design of composites-based adsorbents. Indeed, low grade coal is characterized by the presence of high concentrations of impurities (e.g., the ash content and resinous materials) and, consequently, additional physical and chemical treatments are needed before using this low grade coal in the fabrication of composite materials [7].

Recently, anthracite–based composites were synthetized and utilized to remove organic (methyl orange) and inorganic (manganese and chromate ions) water pollutants [7, 20]. The treatment of anthracite with H_2O_2 (MAn) was suggested to be an effective method to insert different modifiers as chitosan and Fe_3O_4 nanoparticles in the created pores of An structure due to this interface [7, 2]. On the other hand, TiO_2 is widely used to remove organic dyes via either degradation or adsorption due to its chemical stability, biocompatibility, and non-toxicity [17]. Moreover, TiO_2 has a great ability to interact with organic molecules in aqueous solutions [21]. Note that the rutile (Rt) is a titanium oxide mineral (TiO_2) that can be used in water treatment applications. For instance,

polypyrrole/TiO_2 composite, thiazolylazopyrimidine-functionalized TiO_2 nanoparticles, Ag-modified TiO_2 nanotube, poly(p-anisidine)/TiO_2 nanocomposite were applied to remove methylene blue [22], copper ions [23], mercury and cationic dyes [24], respectively. In this study, the utilized Rt was extracted from the Egyptian ilmenite ($FeTiO_3$) and due to the high purity of Rt, it can be used to synthesize novel adsorbents with remaining properties for water depollution especially organic compounds like dyes.

Modeling of the removal data results is required to understand the adsorption mechanism and the physicochemical parameters that could govern it [3]. Generally, Freundlich and Langmuir models are insufficient to understand the uptake mechanism because their parameters lack of a physical meaning [26, 7]. Besides, the fundaments of the common traditional isotherm models (e.g., Langmuir, Freundlich, Sips) are insufficient to describe the adsorption geometry of removed adsorbates [27]. On the contrary case, steric and energetic parameters derived from the advanced statistical physics models can outline microscopically and macroscopically the interactions between the tested pollutants and adsorbents [28, 3, 19]. Consequently, deep and interesting analyses can be resulted from the interpretation of physicochemical parameters obtained with these advanced adsorption models.

The novelty of this study was to synthetize an effective adsorbent for MG dye via inserting Rt nanoparticles prepared from the Egyptian ilmenite ore in the H_2O_2–activated anthracite (MAn). Different techniques (i.e., XRD, FESEM, FTIR) were used in characterizing the Rt/An composite. Freundlich and Langmuir equations were used to correlate the MG adsorption data at 25 – 55 ^{0}C. A statistical physics-based multilayer adsorption model was utilized to provide new evidences and a deeper understanding of the

adsorption interactions between MG molecules and Rt/ MAn active sites. Overall, the MAn impregnated with Rt nanoparticles showed high MG adsorption capacities and it could be extended for the removal of other organic water pollutants. Furthermore, the results of this study contributed with new insights into MG adsorption mechanism using this novel Rt/ MAn composite.

2. Materials and methods

2.1. Materials

Anthracite attained from Marsa Matrouh Company in Egypt was pulverized to get a particle size less than 100 μm. High purity Rutile (Rt) synthesized from ilmenite was obtained via mechanical activation of $FeTiO_3$ followed by reduction, acidic leaching and calcination at 600 ^{0}C/2 h [25]. Rt obtained through this combined process was very pure (i.e., nearly 96 % of TiO_2) without coloring metals [25]. Malachite green ($C_{23}H_{25}N_2$, Sigma-Aldrich, λmax = 617 nm, MW= 364.911 g/mol), hydrogen peroxide (30 %, H_2O_2, Loba Chemie, Pvt, Ltd, Mumbai, India), HCl (0.01 mol/L), NH_4OH (0.01 mol/L) and distilled water were utilized in this study.

2.2. Synthesis of rutile nanoparticles/anthracite (Rt/MAn) adsorbent

H_2O_2-treated anthracite (MAn) was obtained via the addition of 15 mL of H_2O_2 to 3.0 g of the anthracite powder. This anthracite–H_2O_2 mixture was continuously stirred for 60 min at 40 °C. 0.75 g of Rt nanoparticles powder was added to the solution of activated An and stirred for 2 h at 40 °C. Centrifugation for 20 min at 6000 rpm was utilized to separate the solid phase. Final solid was washed with distilled water and dried for 24 h at 70 ^{o}C. Lastly, it was homogenized by agate mortar and stored as Rt/MAn for its further applications.

2.3. Rt/MAn characterization

X–ray diffraction (XRD) analysis of the prepared Rt/ MAn composite was obtained with a X–ray diffractometer (Panalytical Philips APD-3720, Netherlands) with Cu–kα radiation ($\lambda = 0.154$ cm^{-1}) and operated at 40 kV, 35 mA, 5 min scanning speed in the 2θ range of 5 – 80°. Fourier transform infrared (FTIR) spectrum of the Rt/MAn composite was recorded in the range of 400–4000 cm^{-1} with a Bruker FT/IR□2000 spectrometer. Field emission scanning electron microscope (FESEM, Sigma 500 VP, Germany) was employed for studying the morphological features of Rt/MAn composite. pH at the point of zero charge (pH_{PZC}) (i.e., the point at which final pH–initial pH (ΔpH) = zero) was determined as follows [51]: A solution of 0.1 M KCl was prepared and then, 50 mL samples of 0.1 M KCl were taken in beakers. The initial pH (pH_i) of these prepared solutions was separately adjusted at different values ranged from 2.0 to 10.0. Finally, 0.1 g of Rt/MAn composite was added to each beaker and mixed at 200 rpm for 48 h and the final solution pH was measured. Data of ΔpH and initial pH were used for finding the pH_{PZC}.

2.4. Impact of solution pH on the MG adsorption on Rt/MAn

MG adsorption by Rt/MAn composite was studied at different pH values (i.e., 2.0 - 10.0) at 25 ^{0}C where the other adsorption factors remained constant (i.e., 25 mg of Rt/MAn, 100 mg/L of MG concentration, 150 min of shaking time). MG concentrations of all solutions were analyzed with a double beam ultraviolet UV-visible absorption spectrometer (Shimadzu, 1601).

2.5. Equilibrium studies of MG adsorption

Standard MG solutions (1000 mg/L) were prepared and diluted by adding distilled water to reach the needed concentrations for the isotherm experiments. Equilibrium

studies of MG adsorption were performed at pH 8.0 and 25, 40 and 55 °C. MG adsorption isotherms were determined with 25 mL of MG solutions (initial concentrations ranging from 100 to 400 mg/L) and 0.025 g of Rt/MAn composite. In all the equilibrium experiments, the MG Rt/MAn suspensions were mixed for 150 min at 200 rpm via an orbital shaker (SHO 2D shaker, Germany). MG adsorption capacities (q_e mg/g) were obtained via Equation (1).

$$q_e = (C_0 - C_e)\frac{V}{m} \quad (1)$$

where m is the Rt/MAn adsorbent dose (g), V is the MG solution volume (L), C_e and C_0 (mg/L) are the equilibrium and initial MG concentrations, respectively.

2.6. Modeling analysis

Experimental data from MG adsorption onto Rt/MAn were fitted to Langmuir [29] and Freundlich [30] equations as given in Table 1. The best isotherm for describing the experimental results was identified via the values of determination coefficient (R^2) and Chi square (χ^2), see Table 1.

Table 1. Isotherm models used to analyze MG adsorption by Rt/MAn composite.

Isotherm Model	Formula	Parameters	Refs.
Langmuir	$q_e = \frac{q_{\max} K_L C_e}{(1+K_L C_e)}$	C_e (mg/L): equilibrium MG concentration in the aqueous solution q_e (mg/g): MG adsorption capacity at equilibrium. $q_{\max}$ (mg/g): maximum adsorption capacity K_L (L/mg): Langmuir constant	[29]
Freundlich	$q_e = K_F\, C_e^{\,1/n}$	$K_F((\text{mg/g})(\text{mg /L})^{-1/n})$: MG adsorption capacity. n: the heterogeneity factor	[30]

$R^2 = 1 - \frac{\sum(q_{e,\text{exp}} - q_{e,\text{cal}})^2}{\sum(q_{e,\text{exp}} - q_{e,mean})^2}$	$q_{e,\text{exp}}$: Experimental adsorption capacity (mg/g).	[2]
$\chi^2 = \sum \frac{(q_{e,\text{cal}} - q_{e,\text{exp}})^2}{q_{e,\text{exp}}}$	$q_{e,\text{cal}}$: Calculated adsorption capacity (mg/g)	[2]

Theoretically, a statistical physics-based multilayer adsorption model was utilized to fit the MG adsorption on Rt/MAn adsorbent. The appropriateness of this model to fit the MG experimental results was confirmed via the values of R^2 and the root mean square error (RMSE) as the following [2, 18]:

$$\text{RMSE} = \sqrt{\frac{\sum_{i=1}^{m}(Q_{i\,\text{cal}} - Q_{i\,\text{exp}})^2}{m' - p}} \quad (2)$$

Where p is the number of adjustable parameters and m' is the experimental data.

Based on the assumptions of this model, the MG–Rt/MAn interaction was associated to diverse energies, which corresponded to the existence of a limited number of adsorbed MG layers on Rt/MAn composite surface [28, 2]. The main adsorption energy was related to the interaction between the first adsorbed MG layer (stable number) and Rt/MAn active sites, while the further energy was associated to the MG□MG interaction. Therefore, the number of the adsorbed MG layers is equal to $1 + N_2$ [2]. $N_2 = 0$, 1 or > 1, which corresponds to a monolayer ($N_2 = 0$), double□layer ($N_2 = 1$), and multilayer process ($N_2 > 1$) [31].

According to the multilayer adsorption model, several states were suggested as follows: [28, 2]:

- Multilayer adsorption: n and N_2 were adjusted.
- Monolayer adsorption: n was adjusted and $N_2 = 0$.

- ❖ Double-layer adsorption: n was adjusted and N_2 =1.
- ❖ Triple-layer adsorption: n was adjusted and N_2 =2.
- ❖ Langmuir model: $n = 1$ and $N_2 = 0$.

This model is defined by [28, 32].

$$Q = n\, D_M \frac{F_1(c)+F_2(c)+F_3(c)+F_4(c)}{G(c)} \tag{3}$$

$$F_1(c) = -\frac{2\left(\frac{c}{c_1}\right)^{2n}}{1-\left(\frac{c}{c_1}\right)^{n}} + \frac{\left(\frac{c}{c_1}\right)^{n}\left(1-\left(\frac{c}{c_1}\right)^{2n}\right)}{\left(1-\left(\frac{c}{c_1}\right)^{n}\right)^{2}}, \tag{4}$$

$$F_2(c) = \frac{2\left(\frac{c}{c_1}\right)^{n}\left(\frac{c}{c_2}\right)^{n}\left(1-\left(\frac{c}{c_2}\right)^{n\,N_2}\right)}{1-\left(\frac{c}{c_2}\right)^{n}}, \tag{5}$$

$$F_3(c) = -N_2 \frac{\left(\frac{c}{c_1}\right)^{n}\left(\frac{c}{c_2}\right)^{n}\left(\frac{c}{c_2}\right)^{n\,N_2}}{1-\left(\frac{c}{c_2}\right)^{n}}, \tag{6}$$

$$F_4(c) = \frac{\left(\frac{c}{c_1}\right)^{n}\left(\frac{c}{c_2}\right)^{2n}\left(1-\left(\frac{c}{c_2}\right)^{n\,N_2}\right)}{\left(1-\left(\frac{c}{c_2}\right)^{n}\right)^{2}}, \tag{7}$$

$$G(c) = \frac{\left(1-\left(\frac{c}{c_1}\right)^{2n}\right)}{1-\left(\frac{c}{c_1}\right)^{n}} + \frac{\left(\frac{c}{c_1}\right)^{n}\left(\frac{c}{c_2}\right)^{n}\left(1-\left(\frac{c}{c_2}\right)^{n\,N_2}\right)}{\left(1-\left(\frac{c}{c_2}\right)^{n}\right)^{2}}, \tag{8}$$

where D_M is the adsorption sites density of the Rt/MAn adsorbent, n is the number of adsorbed MG molecules per functional group, C_1 and C_2 characterize the half-saturation concentrations (C_1 is associated to the first layer, while C_2 is related to N_2 layers of the adsorbed MG molecules). Also, the parameter N_2 indicates the formation of adsorbed MG layers with a given adsorption energy.

2.7. Regeneration of Rt/MAn adsorbent

Recycling and utilization of any adsorbent several times is an important issue for reducing water treatment costs in industrial processes [8]. Here, adsorption/desorption

tests were repeated 5 times to investigate the reusing of Rt/MAn adsorbent. Desorption of MG dye was achieved using 100 mL of sodium hydroxide (0.5 M) as a desorbing factor. At 25 °C, Rt/MAn composite loaded with MG molecules was agitated for 150 min at 200 rpm using a rotatory shaker. This adsorption/desorption process was repeated five times. Before each desorption stage, the Rt/MAn was extensively washed by distilled water and dried in an electrical oven for 12 h at 70 ^{0}C.

3. Results and discussions

3.1. Rt/MAn characterization

The XRD pattern of Rt/MAn composite shows strong diffraction peaks in the 2θ range between 27^0 and 70^0 (Fig. 1a). The detected peaks had an excellent agreement with the standard JCPDS card no: 88-1175 (space group: $P4_2/mnm$), which confirmed that all of these peaks were related to rutile (TiO_2) nanoparticles. It can be observed that rutile peaks were narrow and sharp, which indicated that Rt was characterized by a high degree of crystallinity. The overlap between the weak anthracite peaks at (0 0 2) and (1 0 0), corresponding to $2\theta=24-29°$ and $42-45°$, and the sharp Rt peaks resulted in the disappearance of the An phase.

FTIR spectrum of the Rt/MAn composite (Fig. 1b) showed the presence of different Ti-O stretching bands between 400 and 1000 cm^{-1} (i.e. the observed bands were at 423, 633 and 891 cm^{-1}) [33, 34]. These peaks could be associated to the Rt nanoparticles. Moreover, the bands at 1562 and 1072 cm^{-1} corresponded to C=C and C=O stretching bands of anthracite, respectively [34-36]. The existence of C=O functional group in MAn sample enhanced its adsorption capacity for both inorganic and organic compounds [36]. Therefore, MG adsorption properties of the MAn were expected to be better than those of

Rt nanoparticles. The additional peaks identified at ~ 3728 and 3794 cm^{-1} were related to the hydroxyl group (–OH) stretching bands [2, 35, 19].

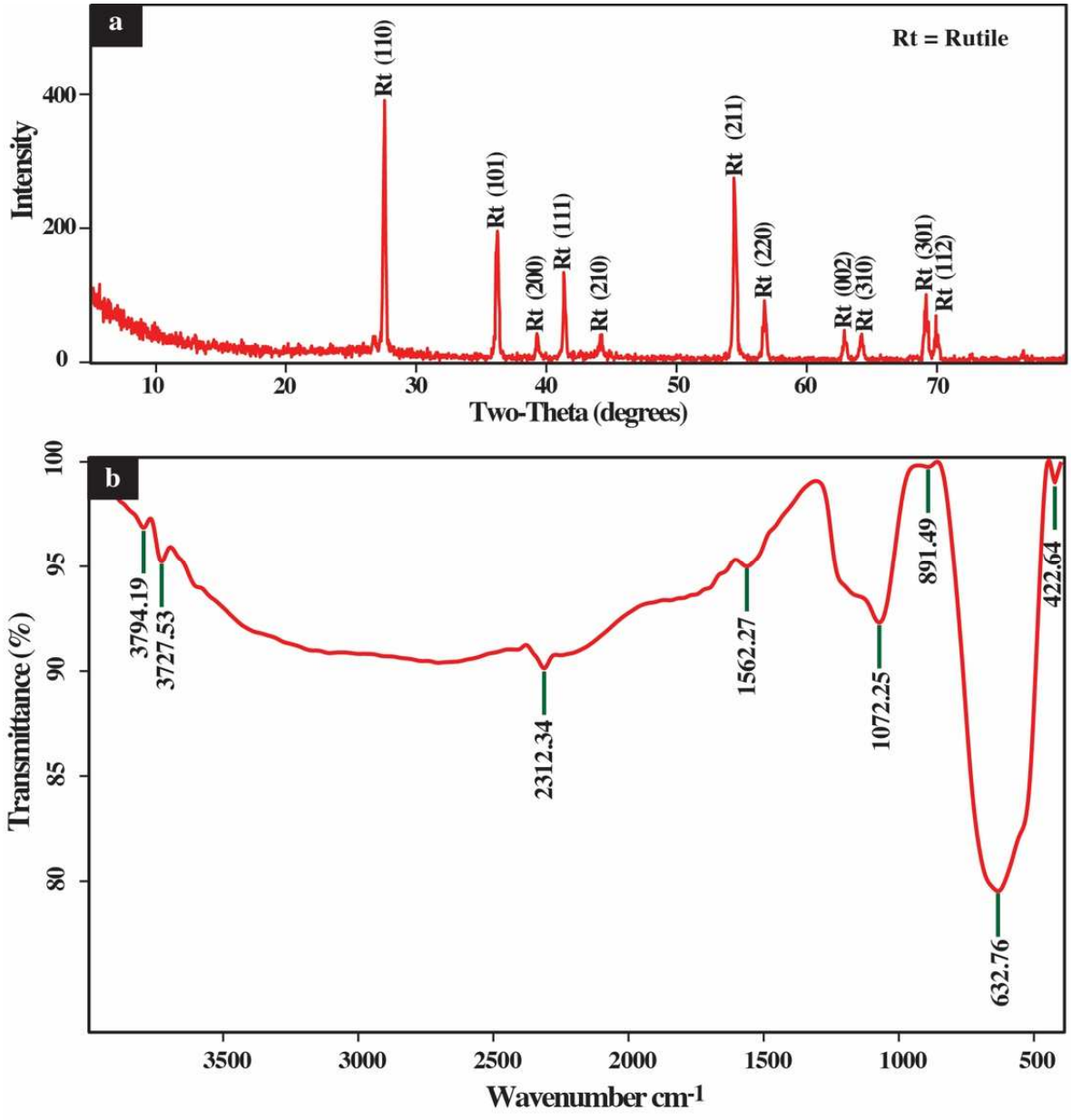

Figure 1. Characterization results of the Rt/MAn composite: (a) XRD pattern and (b) FTIR spectrum.

FESEM results of the Rt/MAn composite (Fig. 2) showed the smooth surface of An with flaky habits due to its internal structure. H_2O_2–activated anthracite (MAn) displayed fissures and pores with dissimilar sizes, diameters and lengths (Fig. 2). Moreover, Rt appeared as agglomerated spherical nanoparticles with different diameters of less than 100 nm (Fig. 2). The presence of these spherical-like TiO_2 nanoparticles could be expected to improve the adsorption of MG molecules due to the increment of Rt/MAn surface area. The Rt nanoparticles were not only attached to the outer anthracite surface, but also were filled the fissures and pores, thus reflecting the physical interface between Rt and Man phases.

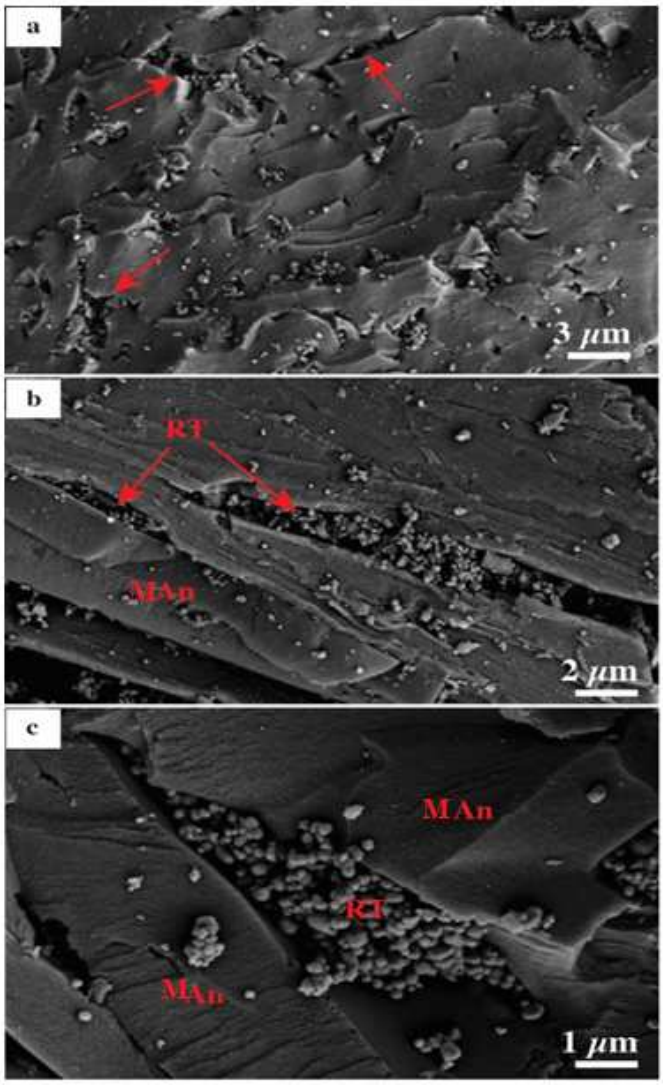

Figure 2. FESEM images of the Rt/MAn composite at different magnifications

3.2. Determination of pH_{PZC} and the pH effect on MG adsorption by Rt/MAn

The pH_{PZC} of this composite was 6.4 (Fig. 3a), which indicated that the MG removal with Rt/MAn was more effective at pH > 6.0. MG adsorption by Rt/MAn composite as function of solution pH is displayed in Figure 3b. MG removal [%] improved by increasing the pH at tested operating conditions thus reaching the maximum removal (i.e., more than

95 %) of MG at pH ≥ 7. This performance (96.2 %) could be linked to the existence of several adsorption sites (functional groups) at Rt/MAn surface, which can be charged at different pH values. Moreover, this performance was found to be higher than that of Rt (71.4 %) and MAn (49.8 %) as individual components at the same pH value (Fig3b). At pH 2.0–3.0, the solutions were characterized by high concentrations of the H^+ thus, the functional groups of Rt/MAn were protonated [37, 9].

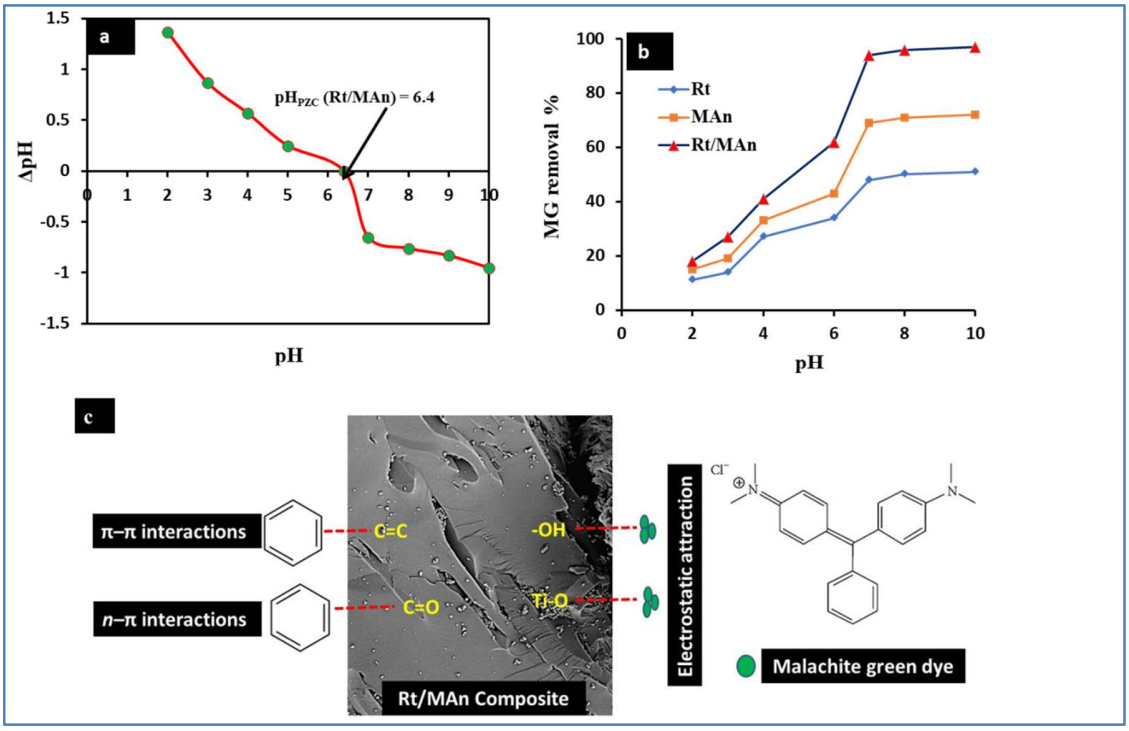

Figure 3. (a) pH $_{ZCP}$ of the Rt/MAn composite, (b) effect of solution pH on the MG removal and (c) the illustration of interaction forces involved in the MG removal by the Rt/MAn composite.

Consequently, the electrostatic repulsion between the positive Rt/MAn functional groups and this cationic dye resulted in decreasing the MG adsorption [8, 37]. At pH 4.0–6.0, the deprotonation of the Rt/MAn surface enhanced the MG removal (i.e., a decrease of protons was distinguished) [14]. However, it can observed that the Rt/MAn composite can

remove MG molecules at pH 2.0–6.0, which could be related to the complexation with oxygen–holding functionalities [7]. Furthermore, the involvement of π–π and n–π interactions due to the existence of C=C and C=O groups in the pure MAn contributed to improve the dye adsorption by the MAn sample as compared to Rt nanoparticles [38], see Figure 3c. At pH ≥ 7.0, the strong interaction between the deprotonated surface functionalities of Rt/MAn and dye molecules greatly improved the removal process and consequently, all the equilibrium MG removal experiments were conducted at solution pH 8.0.

3.3. MG adsorption isotherms (traditional and advanced modeling)

Experimental adsorption isotherms were correlated with Freundlich, Langmuir and the statistical physics multilayer models. The adjustable parameters of these models were calculated and interpreted in the coming subsections.

The relation between q_e and C_e (Fig. 4) was applied to define the parameters of the Freundlich and Langmuir equations as given in Table 2. At all tested temperatures, the two classical models fitted well the MG adsorption by the Rt/MAn composite where R^2 was close to unity. Statistical analysis of these models was complemented with the Chi–squared (χ^2). The Freundlich model presented the lowest Chi–squared values at all tested conditions in comparison to the Langmuir model. Freundlich equation was the best isotherm and, thus the adsorption of MG molecules was associated to an heterogeneous surface of Rt/MAn composite with different active sites. The maximum Langmuir monolayer adsorption capacities (q_{max}) improved with temperature (Table 2). Consequently, the interaction between Rt/MAn composite and MG dye was more effective with increments of solution temperature. Similarly, K_F of Freundlich equation ranged from

34.28 to 41.21 $(mg/g)(mg/L)^{-1/n}$ where solution temperature increased from 25 to 55 °C thus confirming the endothermic nature of MG adsorption.

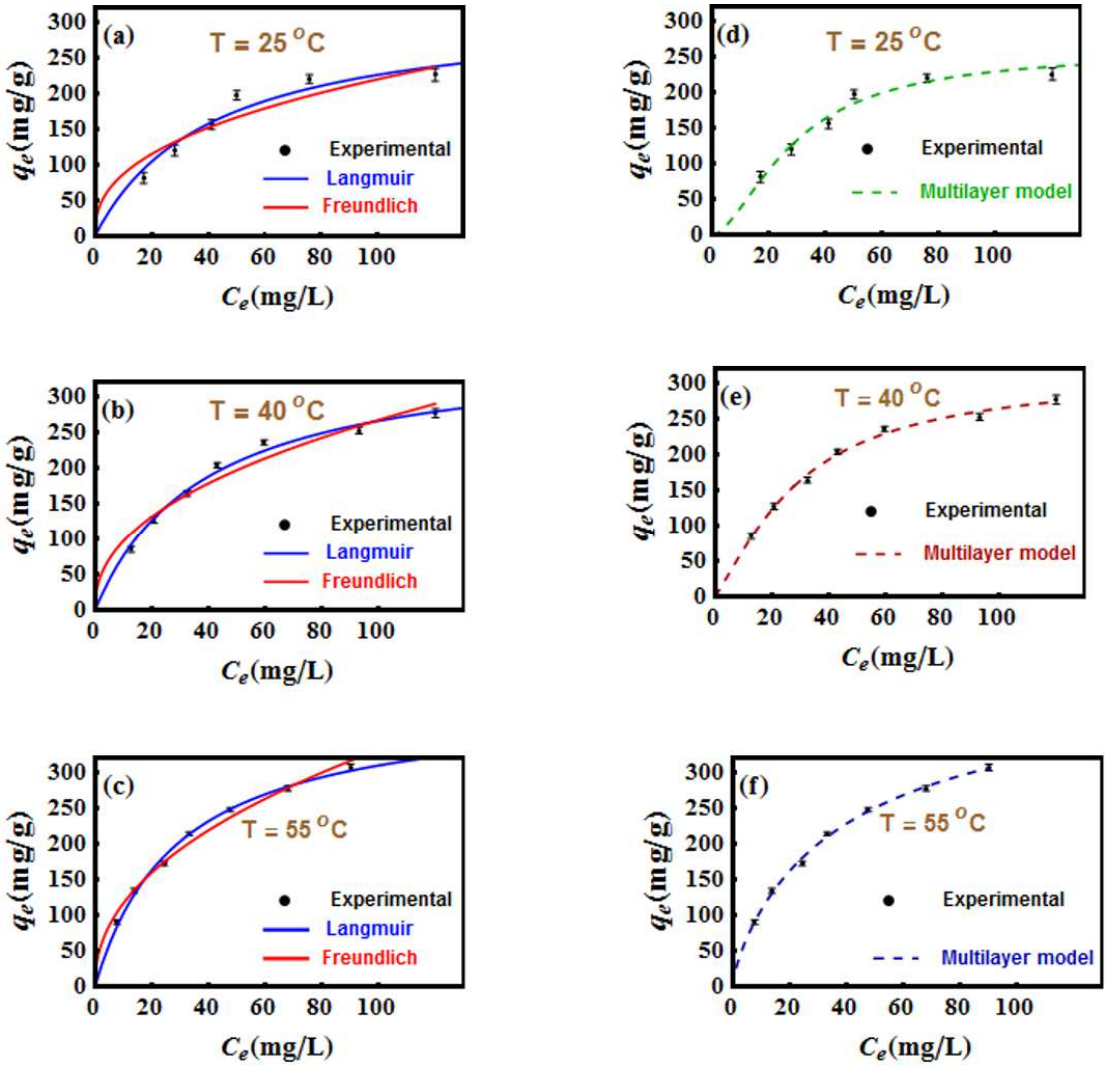

Figure 4. Experimental adsorption isotherms of MG adsorption on Rt/MAn composite at 25 - 55^{0}C and their correlation with Langmuir, Freundlich and the statistical physics multilayer adsorption models.

Note that the mobility of MG molecules increased at higher adsorption temperatures, which resulted in the improvement of the interactions between MG molecules and Rt/MAn active sites. A similar result was reported by previous articles [7, 2,

19]. In addition, the $1/n$ values (Table 2) were less than 1.0 thus indicating an effective MG adsorption even at low concentrations.

Table 2. Parameters of isotherm equations for the MG adsorption on Rt/MAn composite.

Isotherm Model	25 °C	40 °C	55 °C
Langmuir			
q_{max} (mg/g)	320.03	368.14	400.27
k_L (L /mg)	0.024	0.026	0.035
R^2	0.9893	0.9942	0.9983
χ^2	2.2	1.89	1.65
Freundlich			
k_F ((mg/g)(mg /L)$^{-1/n}$)	34.28	35.09	41.21
$1/n$	0.404	0.44	0.453
R^2	0.9956	0.9988	0.9994
χ^2	1.82	1.57	1.24
Multilayer			
Q_{sat} (mg/g)	531.3	690.4	739.6
R^2	0.998	0.9994	0.9997
RMSE	1.8	0.891	0.572

Maximum adsorption capacities (q_{max}) of MG for different adsorbents as compared to the Rt/MAn performance were collected in Table 3. These results indicated that the Rt/MAn composite prepared in this study outperformed several adsorbents and this novel material is an interesting alternative to remove MG from wastewaters at industrial level.

Table 3. MG adsorption capacities for natural and synthetic materials and their comparison with Rt/MAn composite.

Adsorbent	Adsorption capacity q_{max} (mg/g)	Reference
Bentonite	179	[12]
Activated carbon	57.14	[15]
Neem sawdust	4.35	[39]
Rattan sawdust	62.7	[40]
Carbon	8.44	[14]
Halloysite nanotubes	99.6	[10]
Natural zeolite	23.94	[13]
Modified rice husk	12.16	[16]
Degreased coffee bean	55.3	[41]
Treated ginger waste	84.03	[42]
Diatomite	23.64	[43]
Modified carbon nano tubes	172	[44]
Cellulose nanofibril aerogels	212.7	[45]
Graphene oxide/Fe_3O_4	179	[46]
NiO nano-flakes	142	[47]
Rt/MAn composite	320.03	The present study
Rt/MAn (theoretical)	531.3	The present study

On the other hand, the interpretation of the interactions between the removed MG molecules and the Rt/MAn active sites via statistical physics calculations is a reliable approach to understand the corresponding adsorption mechanism [48,49]. MG–Rt/MAn interaction was mainly governed by different physicochemical parameters that can set-up the adsorption mechanism. Consequently, the steric parameters (i.e., n, D_M, N_t, and the saturation adsorption capacities of MG dye ($Q_{sat} = n.\ DM.\ Nt$) were determined. Adsorption energies (ΔE) associated to this removal process were also calculated.

The theory of the multilayer adsorption model was utilized to examine these physicochemical and energetic parameters [49,50]. The highest R^2 and the lowest RMSE values indicated that the employed multilayer model is adequate for representing the MG adsorption results, see Figure 4 and Table 2.

3.4. Steric parameters

Based on the previous studies, the n parameter was utilized to correct the assumption of the Langmuir model [26, 1, 2, 19]. Note that $n = 1$ (i.e., Langmuir hypothesis), $n > 1$ or $n < 1$, which reveals dissimilar adsorbent performances. This parameter can also explain the position (i.e., vertical or horizontal) of the adsorbed MG molecules on Rt/MAn surface. For instance, the parameter $n > 1$ or < 1 indicated the vertical or horizontal position of the adsorbed MG molecules, respectively. Moreover, the MG adsorption mechanism for Rt/MAn composite could be multi–docking (i.e., several Rt/MAn active sites can remove one MG molecule if $n < 1$) or multi–molecular (one functional group of this adsorbent can bind several MG molecules when n > 1) [1, 2, 19]. Figure 5a shows the parameter n versus the adsorption temperature. The parameter n was 1.60, 1.36 and 0.96 at 25, 40 and 55 ^{0}C (i.e., n offered different adsorption scenarios with respect to the aqueous solution temperature). At 25 and 40 ^{0}C, the multi–interactions mechanism and vertical adsorption position were linked to the interface between MG molecules and Rt/MAn active sites. On the contrary case, a multi–docking mechanism and horizontal adsorption geometry were associated to the MG-Rt/MAn interaction at 55 ^{0}C. Thus, the aggregation of MG molecules in solution (i.e., MG-MG binding), especially at the first temperature, was an important factor for the occurrence of the vertical (non-parallel) position and the multi–interactions mechanism. The increment of solution temperature

decreased n value up to < 1.0 at the final temperature and therefore, the temperature affected the interaction between MG molecules for the formation of molecular aggregates in the aqueous solution. The low degree of MG aggregation at 55 ^{0}C indicated that the Rt/MAn surface could imply a fast remove of this dye at different functional groups of this adsorbent before its aggregation in solution.

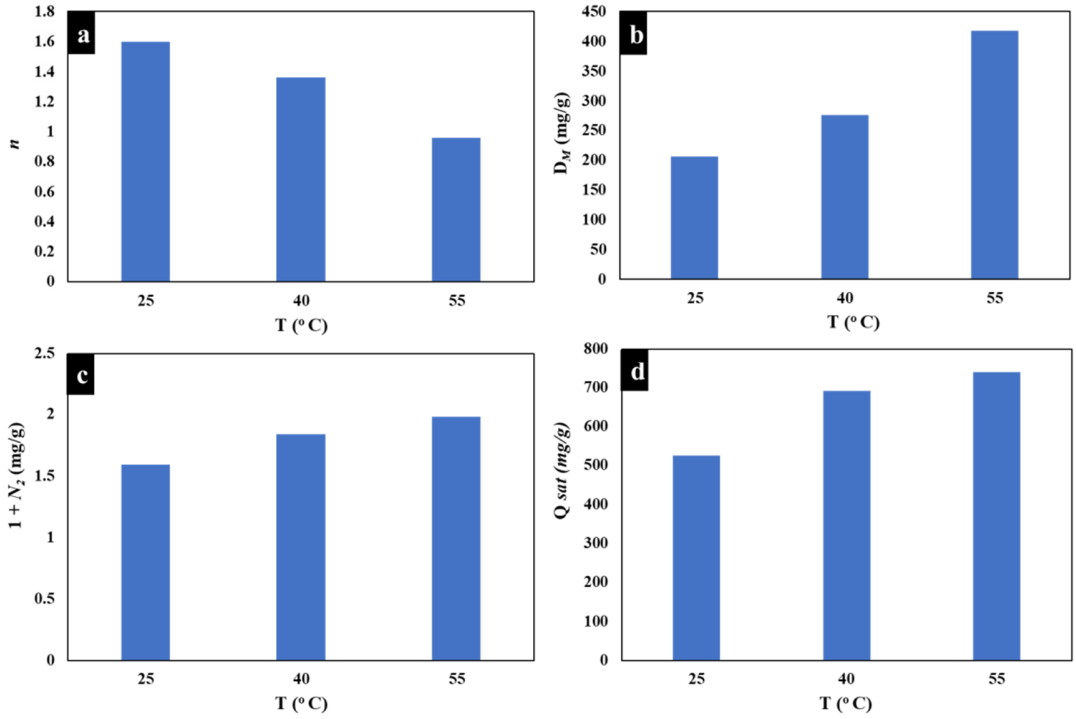

Figure 5. Calculated physicochemical parameters n, N_M, , N_t, and Q_{sat} as function of temperature for MG adsorption on the Rt/MAn composite.

Also, the chemical stability of molecular aggregates is highly dependent of solution temperature where increments in this operating parameter reduce the dye molecular aggregation.

Concerning the density of Rt/MAn active sites (D_M), the increment of adsorption temperature from 25 to 55 °C (Fig. 5b) caused an enhancing of this parameter from 206.25 to 417.48 mg/g. The increase of this physicochemical parameter with temperature was

chiefly associated to the involvement of new sites of Rt/MAn composite in the removal of MG molecules. Certainly, the aggregation of the MG molecules at the initial temperature (25 ^{0}C) can hide some active sites of Rt/MAn composite. With increasing the solution temperature to the value of 55 °C, the aggregation of MG molecules decreased and thus, more receptors sites of Rt/MAn are occupied. Generally, the parameter D_M displayed an opposite trend than that identified for the parameter n (i.e., n and D_M showed conflicting trends with adsorption temperature).

Determination of the total removed layers is necessary to better understand the adsorption mechanism of the adsorbate MG molecules onto the investigated Rt/An composite. The calculated total number of formed MG layers ($N_t = 1 + N_2$) was ~ 2.0 at all temperatures (Fig. 5c). Thus, the temperature showed a reduced impact on this parameter during the MG adsorption at tested operating conditions. So, the mechanism of MG adsorption onto Rt/MAn based on the N_t parameter could be ignored.

The values corresponding to the saturation adsorption capacity can clarify the efficacy of Rt/MAn adsorbent to remove MG molecules. Q_{sat} was 531.30, 690.40 and 739.60 mg/g at 25, 40 and 55 °C, respectively, see Figure 5d. Enhancing the MG adsorption capacity with increasing temperature could be linked to the high mobility of the dye molecules at higher temperatures [2, 3]. Thus, the unrestricted MG molecules can interact with new active sites of the Rt/MAn adsorbent causing increasing the adsorption capacities at 40 and 55 °C. Moreover, the attained Q_{sat} values confirmed the endothermic nature of the interaction between the MG molecules and Rt/MAn adsorption sites. It was noticed that Q_{sat} and D_M displayed the same trend (i.e., they increased significantly with temperature), which reflected that the parameter D_M was considered as the main factor that affected the

adsorption efficiency of Rt/MAn composite. Furthermore, the result of ($n.D_M$) values (i.e., the N_2 value was supposed to be zero) was close to the adsorption capacities of Langmuir model, which indicated that the experimental and theoretical data were consistent.

3. 5. Energetic parameters

To attain a suitable interpretation of the interface between MG molecules and Rt/MAn active sites, determination of the adsorption energies is obligatory [3]. The multilayer adsorption energies (ΔE) were calculated with the next equations [2].

$$C_1 = C_s e^{-\frac{\Delta E_1}{RT}} \quad (9)$$

$$C_2 = C_s e^{-\frac{\Delta E_2}{RT}} \quad (10)$$

where $c_1$and c_2 denote to the half-saturation concentrations and c_s is the solubility of the tested adsorbate.

Figure 6a shows calculated ΔE versus adsorption temperature. The positive ΔE (i.e., ΔE_1 and $\Delta E_2 > 0$) confirmed the endothermic interaction between the MG dye molecules and Rt/MAn adsorbent. In addition, all ΔE values were < 40 kJ/mol where physical adsorption forces contributed in the interface between MG adsorbate and Rt/MAn adsorbent. $\Delta E_1 > \Delta E_2$ at all tested temperatures, see Fig. 6a. As stated, ΔE_1 corresponded to Rt/MAn–MG interaction, while ΔE_2 characterized the MG–MG interaction and, consequently, ΔE_1 values were higher than ΔE_2.

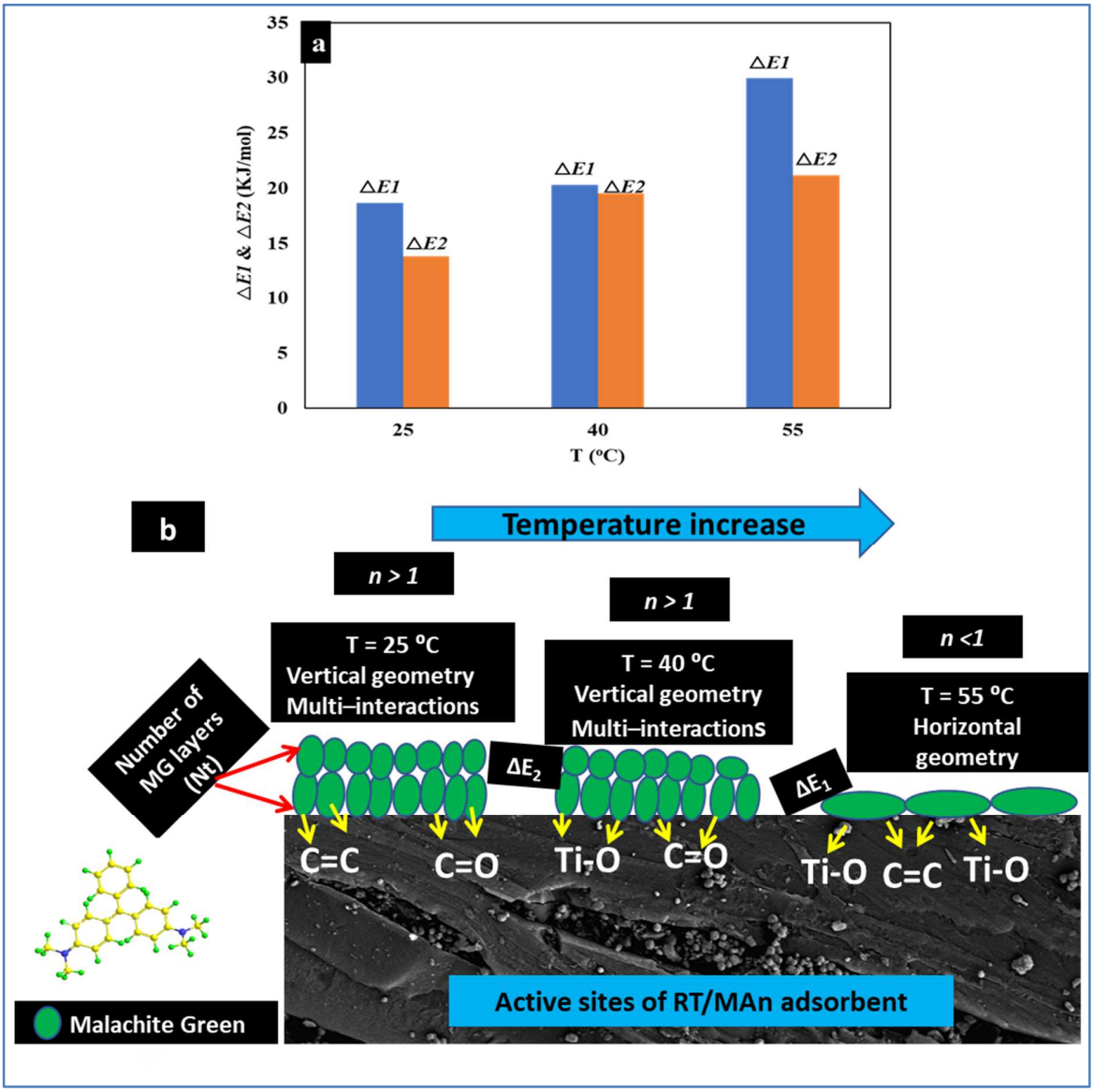

Figure 6. (a) Calculated adsorption energies (ΔE) and (b) the description of MG adsorption mechanism based on the statistical physics multilayer model.

Also, the trend of ΔE versus temperature could be associated to the improvement of MG adsorption capacities (i.e., Q_{sat} and ΔE showed the same trends). Overall, the adsorption mechanism of MG dye was governed by the energetic (ΔE) and steric (D_M) parameters. The probable adsorption mechanism of MG molecules onto the Rt/MAn composite is illustrated in Figure 6b.

3.6. Reusability Study

Figure 7 indicates that the Rt/MAn composite showed more than 80 % of MG removal after all regeneration cycles. Therefore, this novel adsorbent can be reutilized several times to adsorb dye MG without an important loss of its efficiency, thus signifying an economic benefit and high stability of this adsorbent in water treatment.

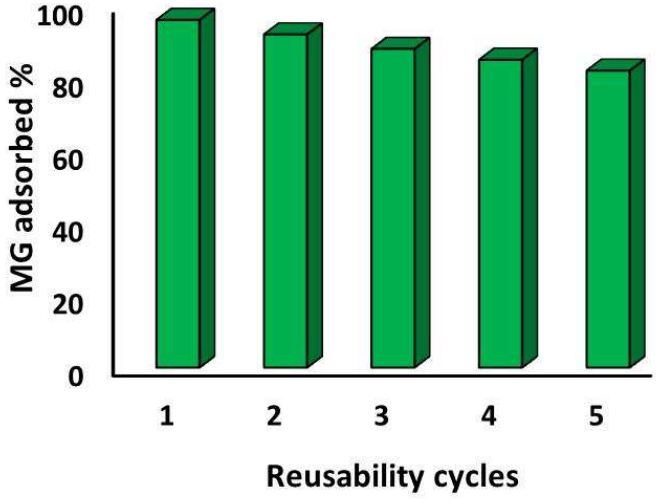

Figure 7. MG removal after the regeneration of Rt/MAn composite

Two possible reasons could be responsible for the slight decrease of adsorption capabilities of the Rt/MAn composite [8]: (I) irreversible adsorption of MG dye molecules that could limit their desorption and (II) the slow elimination of surface chemistry and porosity of the Rt/MAn adsorbent (including water-driven processes in adsorption cycles and NaOH-driven in the desorption runs) due to the treatment applied for the regeneration process.

Finally, utilizing natural materials (e.g., coal, clays, lignite) or industrial/and or agricultural by-products (e.g., pomegranate peel, silica fume, fly ash, iron slag) in the synthesis of adsorbents is desired due to the low-cost and the availability of these

materials. Regarding the investigated composite, Rt/MAn adsorbent was fabricated using rutile nanoparticles extracted from Egyptian ilmenite mineral and hard coal through a simple and cost-effective technique. Based on the adsorption and desorption results, Rt/MAn is recommended to be a promising adsorbent for decontamination of MG-bearing solutions.

4. Conclusions

A new adsorbent (Rt/MAn) was synthesized using rutile nanoparticles and treated anthracite via a simple and low-cost technique. Results of XRD, FESEM and FTIR confirmed the insertion of Rt (TiO_2) to the structure of An sample. The Rt/MAn composite was utilized as adsorbent of MG dye at 25 - 55 °C. Calculations performed with a statistical physics-based multilayer adsorption model suggested that multi-interactions mechanisms and multi-docking could occur in the removal of this dye molecule. The saturation adsorption capacity increased with temperature and this steric parameter was mainly controlled by the number of Rt/MAn active sites. Dye aggregation in the aqueous solution was also present especially at low adsorption temperature. MG removal by Rt/MAn adsorbent was endothermic and associated to physical forces. Results of regeneration study indicated that this novel composite showed a MG removal $>$ 80 % after five cycles of adsorption and desorption. This adsorbent can be utilized in the treatment of industrial wastewaters polluted by this dye. In fact, it can be expected that carbon-rich materials containing rutile nanoparticles will be effective adsorbents to remove organic pollutants in wastewater remediation.

Acknowledgements

The authors would like to thank the STDF unit, Egypt, to financially support this article (The project number: 25552).

References

[1] Z. Li, G. Wang, K. Zhai, C. He, Q. Li, P. Guo. Methylene blue adsorption from aqueous solution by loofah sponge-based porous carbons. Colloids Surf. A Physicochem. Eng. Asp. 538 (2018) 28-35.

[2] M.A. Barakat, A.Q. Selim, M. Mobarak, R. Kumar, I. Anastopoulos, D.A. Giannakoudakis, A. Bonilla-Petriciolet, E.A. Mohamed, M.K.Seliem, S. Komarneni. Experimental and theoretical studies of methyl orange uptake by Mn□rich synthetic mica: Insights into manganese role in adsorption and selectivity. Nanomaterials 10 (2020) 1-19.

[3] M. Atrous, L. Sellaoui, M. Bouzid, E.C. Lima, P.S. Thue, A. Bonilla-Petriciolet, A. Ben Lamine. Adsorption of dyes acid red 1 and acid green 25 on grafted clay: Modeling and statistical physics interpretation. J. Mol. Liq. 294 (2019) 111610.

[4] A.E. Pirbazari, E. Saberikhah, N.G.A. Gorabi. Fe3O4 nanoparticles loaded onto wheat straw: an efficient adsorbent for Basic Blue 9 adsorption from aqueous solution. Desalination and Water Treatment 57 (2014) 4110-4121.

[5] Chen, F., Wu X., X. R. Bu, R., F. Yang. Co–Fe hydrotalcites for efficient removal of dye pollutants via synergistic adsorption and degradation, RSC Advances, 7 (2017) 41945–41954.

[6] G. Wang, Y. Hua, X. Su, S. Komarneni, S. Ma, Y. Wang, Cr(VI) adsorption by montmorillonite nanocomposites. Applied Clay Science 124-125 (2016) 111-118.

[7] E. A. Mohamed, A. Q. Selim, S. A. Ahmed, L. Sellaou, A. Bonilla-Petriciolet, A. Ertoe, Z. Li, Y. Li, M. K. Seliem. H_2O_2–activated anthracite impregnated with chitosan as a novel

composite for Cr(VI) and methyl orange adsorption in single–compound and binary systems: Modeling and mechanism interpretation. Chemical Engineering Journal 380 (2020) 122445.

[8] M.K. Seliem, M. Barczak, I. Anastopoulos, D.A. Giannakoudakis. A Novel Nanocomposite of Activated Serpentine Mineral Decorated with Magnetic Nanoparticles for Rapid and Elective Adsorption of Hazardous Cationic Dyes: Kinetics and Equilibrium Studies, Nanomaterials 10 (2020) 1-12.

[9] M.A. Barakat, R. Kumar, E.C. Lima, M.K. Seliem. Facile synthesis of muscovite–supported Fe_3O_4 nanoparticles as an adsorbent and heterogeneous catalyst for effective removal of methyl orange: Characterisation, modelling, and mechanism. Journal of Taiwan Institute of Chemical Engineers 119 (2021) 146-157.

[10] G. Kiani, M. Dostali, A. Rostami, A.R. Khataee. Adsorption studies on the removal of Malachite Green from aqueous solutions onto halloysite nanotubes. Applied Clay Science 54 (2011) 34-39.

[11] S.Z. Mohammadi, M.A. Karimi, S.N. Yazdy, T. Shamspur, H. Hamidian. Removal of Pb(II) ions and Malachite green dye from wastewater by activated carbon produced from lemon peel. Quimica Nova 5 (2014) 804-809.

[12] E. Bulut, M. Özacar, İ.A. Şengil. Adsorption of malachite green onto bentonite: Equilibrium and kinetic studies and process design. Microporous and Mesoporous Materials 115 (2008) 234-246.

[13] R. Han, Y. Wang, Q. Sun, L. Wang, J. Song, X. He, C. Dou. Malachite green adsorption onto natural zeolite and reuse by microwave irradiation. Journal of Hazardous Materials 175 (2010) 1056-1061.

[14] J. Zhang, Y. Li, C. Zhang, Y. Jing. Adsorption of malachite green from aqueous solution onto carbon prepared from Arundo donax root. Journal of Hazardous Materials 150 (2008) 774-782.

[15] I.A. Rahman, B. Saad, S. Shaidan, E.S. S. Rizal. Adsorption characteristics of malachite green on activated carbon derived from rice husks produced by chemical–thermal process. Bioresource Technology 96 (2005) 1578-1583.

[16] S. Chowdhury, R. Mishra, P. Saha, P. Kushwaha. Adsorption thermodynamics, kinetics and isosteric heat of adsorption of malachite green onto chemically modified rice husk. Desalination 256 (2011) 159-168.

[17] Z.M. Abou-Gamra, M.A. Ahmed. TiO_2 Nanoparticles for Removal of Malachite Green Dye from Waste Water. Scientific Research Publishing 5 (2015) 373-388.

[18] M. Mobarak, E.A. Mohamed, A.Q. Selim, F.M. Mohamed, L. Sellaoui, A.B. Petriciolet, M.K. Seliem. Statistical physics modeling and interpretation of methyl orange adsorption on high–order mesoporous composite of MCM–48 silica with treated rice husk. Journal of Molecular Liquids 285 (2019) 678-687.

[19] H.S. Ramadan, M. Mobarak, E.C. Lima, A. Bonilla-Petriciolet, Z. Li, M.K. Seliem. Cr(VI) adsorption onto a new composite prepared from Meidum black clay and pomegranate peel extract: Experiments and physicochemical interpretations. Journal of Environmental Chemical Engineering 9 (2021) 105352.

[20] M. K. Seliem, M. Mobarak, A. Q. Selim, E. A .Mohamed, R. A. Halfaya, H. K.Gomaa, I. Anastopoulos, D. A. Giannakoudakis, E. C. Lima, A. Bonilla-Petriciolet, G. Luiz Dotto. A novel multifunctional adsorbent of pomegranate peel extract and activated

anthracite for Mn(VII) and Cr(VI) uptake from solutions: Experiments and theoretical treatment. Journal of Molecular Liquids 311 (2020) 113169.

[21] A.G. Thomas, K.L. Syres. Adsorption of organic molecules on rutile TiO_2 and anatase TiO_2 single crystal surfaces. Chemical Society Reviews 41 (2012) 4207-4217.

[22] J. Li, J. Feng, W. Yan. Excellent adsorption and desorption characteristics of polypyrrole/TiO_2 composite for Methylene Blue. Applied Surface Science 279 (2013) 400-408.

[23] Z. Ghasemi, A. Mohammadi. Sensitive and selective colorimetric detection of Cu (II) in water samples by thiazolylazopyrimidine-functionalized TiO2 nanoparticles. Spectrochimica Acta Part A: Molecular and Biomolecular Spectroscopy 239 (2020) 118554

[24] C-Y. Tsai, C-W. Liu, H-C. Hsi, K-S. Lin, Y-W. Lin, L-C. Lai. Synthesis of Ag-modified TiO2 nanotube and its application in photocatalytic degradation of dyes and elemental mercury. Journal of Chemical Technology and Biotechnology 94 (2019) 3251-3262.

[25] M.G. Shahien, M.M.H. Khedr, A.E. Maurice, A.A. Farghali, R.A.M. Ali. Synthesis of high purity rutile nanoparticles from medium-grade Egyptian natural Ilmenite. Beni-Suef University Journal of Basic and Applied Sciences 4 (2015) 207-213.

[26] L. Sellaoui, D.I. Mendoza-Castillo, H.E. Reynel- Ávila, B.A. Ávila-Camacho, H. Ghalla, A. Bonilla-Petriciolet, A. Ben Lamine. Understanding the adsorption of Pb^{2+}, $Hg^{2+}$and Zn^{2+} from aqueous solution on a lignocellulosic biomass char using advanced statistical physics models and density functional theory simulations. Chemical Engineering Journal 365 (2019) 305-316.

[27] M.K. Seliem, M. Mobarak. Cr(VI) uptake by a new adsorbent of CTAB–modified carbonized coal: Experimental and advanced statistical physics studies. Molecular Liquids Journal 294 (2019) 111676.

[28] Z. Li, L. Sellaoui, G.L. Dotto, A.B. Lamine , A.B. Petriciolet , H. Hanafy, H. Belmabrouk, S.N Matias, A. Erto. Interpretation of the adsorption mechanism of Reactive Black 5 and Ponceau 4R dyes on chitosan/polyamide nanofibers via advanced statistical physics model. Journal of Molecular Liquids 285 (2019) 165-170.

[29] I. Langmuir The constitution and fundamental properties of solids and liquids. Journal of American Chemical Society 38 (1916) 2221–2295.

[30] H. M. F. Freundlich. Over the adsorption in solution. Journal of Physical Chemistry 57 (1906) 385-471.

[31] Z. Li, H. Hanafy, L. Zhang, L. Sellaoui, M. S. Netto, M. L. S. Oliveira, M. K. Seliem, G. L. Dotto, A. Bonilla-Petricioleti, Q. Li. Adsorption of Congo red and methylene blue dyes on an ashitaba waste and a walnut shell-based activated carbon from aqueous solutions: Experiments, characterization and physical interpretations. Chemical Engineering Journal 388 (2020) 1-10.

[32] S.F. Azha, M.S. Shamsudin, M. Shahdat, S. Ismail. Low cost zwitterionic adsorbent coating for treatment of anionic and cationic dyes. Journal of Industrial and Engineering Chemistry 67 (2018) 187-198.

[33] N. Nolan, S. Pillai, M. Seery. Spectroscopic Investigation of the Anatase-to-Rutile Transformation of Sol-Gel Synthesised TiO2 Photocatalysts. Journal of Physical Chemistry C, 113 (2009) 16151-16157.

[34] S. El-Sherbiny, F. Morsy, M. Samir, O.A. Fouad. Synthesis, characterization and application of TiO2 nanopowders as special paper coating pigment. Applied Nanosciences 4 (2013) 305-313.

[35] N.A. Akbar, H.A. Aziz, M.N. Adlan. The Characteristics of Limestone and Anthracite Coal as Filter Media in Treating Pollutants from Groundwater. International Journal of Environmental Science and Development 12 (2021) 58-62.

[36] X. Shi, H. Fu, Y. Li, J. Mao, S. Zheng, and D. Zhu. Impact of coal structural heterogeneity on the nonideal sorption of organic contaminants. Environmental Toxicology and Chemistry 30 (2011) 1310-1319.

[37] M.K. Seliem, S. Komarneni. Equilibrium and kinetic studies for adsorption of iron from aqueous solution by synthetic Na-A zeolites: Statistical modeling and optimization. Micropor. Mesopor. Mater. 228 (2016) 266–274.

[38] A.Q. Selim, E.A. Mohamed, M.K. Seliem. Deep insights into the organic carbon role in selectivity and adsorption T mechanism of phosphate and crystal violet onto low–cost black limestone: Modeling and physicochemical parameters interpretation. Colloids and Surfaces A 580 (2019) 123755.

[39] S.D. Khattria, M.K. Singh. Removal of malachite green from dye wastewater using neem sawdust by adsorption. Journal of Hazardous Materials 167 (2009) 1089–1094.

[40] B.H. Hameed, M.I. El-Khaiary. Malachite green adsorption by rattan sawdust: Isotherm, kinetic and mechanism modeling. Journal of Hazardous Materials 159 (2008) 574 – 579.

[41] M. Baek, C.O. Ijagbemi, S. Jin, D. Kim. Removal of malachite green from aqueous solution using degreased coffee bean. Journal of Hazardous Materials 176 (2010) 820–828.

[42] R. Ahmad, R. Kumar. Adsorption studies of hazardous malachite green onto treated ginger waste, Journal of Environmental Management 91 (2010) 1032–1038.

[43] L. Tian, J. Zhang, H. Shi, N. Li, Q. Ping. Adsorption of malachite green by diatomite: equilibrium isotherms and kinetics studies. J. Dispers. Sci. Technol. 37 (2016) 1059-1066.

[44] A. Awadallah-F. Adsorptive removal of malachite green chloride and reactive red- 198 from aqueous solutions by using multiwall carbon nanotubes-graft-poly (2-acrylamido-2-methyl-1-propanesulfonic acid). J. Polym. Environ. 25 (2017) 258-276.

[45] F. Jiang, D.M. Dinh, Y.L. Hsieh. Adsorption and desorption of cationic malachite green dye on cellulose nanofibril aerogels. Carbohydr. Polym. 173 (2017) 286-294.

[46] M.S. Raghu, K. Yogesh Kumar, M.K. Prashanth, B.P. Prasanna, R. Vinuth, C.B. Pradeep Kumar. Adsorption and antimicrobial studies of chemically bonded magnetic graphene oxide-Fe3O4 nanocomposite for water purification. J. Water Process Eng. 17 (2017) 22-31.

[47] A. Wei, B. Liu, H. Zhao, Y. Chen, W. Wang, Y. Ma, H. Yang, S. Liu. Synthesis and formation mechanism of flower like architectures assembled from ultrathin NiO nanoflakes and their adsorption to malachite green and acid red in water. Chem. Eng. J. 239 (2014) 141-148.

[48] A. Gómez-Avilés, L. Sellaoui, M. Badawi, A. Bonilla-Petriciolet, J. Bedia, C. Belver, Simultaneous adsorption of acetaminophen, diclofenac and tetracycline by organo-sepiolite: Experiments and statistical physics modelling, Chem. Eng. J. 404 (2021) 126601.

[49] L. Sellaoui, L.F.O. Silva, M. Badawi, J. Ali, N. Favarin, G.L. Dotto, A. Erto, Z. Chen, Adsorption of ketoprofen and 2- nitrophenol on activated carbon prepared from winery wastes: A combined experimental and theoretical study, J. Mol. Liq. 333 (2021) 115906.

[50] L. Sellaoui, Z. Li, M. Badawi, G.L. Dotto, A. Bonilla-Petriciolet, Z. Chen, Origin of the outstanding performance of Zn–Al and Mg–Fe layered double hydroxides in the adsorption of 2-nitrophenol: a statistical physics assessment, J. Mol. Liq. 314 (2020) 113572.

[51] N. Fiol, I. Villaescusa, Determination of sorbent point zero charges: usefulness in sorption studies. Environmental Chemistry Letters 7 (2009) 79-84.